ADV MATH SCI JOURNAL
Advances in Mathematics: Scientific Journal **11** (2022), no.4, 275–299
ISSN: 1857-8365 (printed); 1857-8438 (electronic)
https://doi.org/10.37418/amsj.11.4.1

EXPERIMENTAL AND 3D NUMERICAL SIMULATION OF THREE SOLAR PONDS WITH DIFFERENT LEVEL OF TURBIDITY: DOUGLAS-GUNN ADI APPROACH

BAHI OUSSAMA[1] AND ABDELLI AMMAR

ABSTRACT. In most previous works dealing with the modelling and numerical simulation of salinity gradient solar ponds, the heat diffusion is 1D or 2D, the diffusion of salt is very slow and that there are small convection movements, which obviously supposes that the wind speed is negligible. The studies are often limited to sodium chloride-based ponds where only relatively clear water is considered. The present work comes to fulfil the lack of 3D thermal behaviour prediction where, in one hand, we simulated solar ponds by a mixture of three different techniques, which are stable and well adapted to this type of problem using the method of finite differences in conjunction with the schemes of ADI-Gunn, Adams-Bashford and Schneider and al, which finds its first application in this type of problems. On the other hand, in order to validate our numerical results, we conducted an experiment on three identical parallelepiped ponds with 2.3040 m^2 of area and 1.200 m depth; each one containing the same fungicide salt namely KH_2PO_4, that has never been used before.

[1]*corresponding author*
2020 *Mathematics Subject Classification.* 76-10.
Key words and phrases. Solar pond, fungicide salt, turbidity, convection, temperature distribution.
Submitted: 10.03.2022; *Accepted:* 28.03.2022; *Published:* 02.04.2022.

1. INTRODUCATION

The technology of solar ponds was discovered by Von-Kalecsinsky in 1902. He observed lakes where a freshwater layer is superimposed on another denser and warmer layer [1]. Since, the idea to artificially create salinity gradient solar ponds has begun. The depletion of fossil fuels with their related pollution problems has led many scientists to conduct studies and investigations on this topic. Several works have shown that it is possible to use the solar energy by transforming it into different forms: (electrical, thermal, chemical,...). Despite this availability, solar energy could not replace traditional energy sources due to the high cost of storage [2]. Salinity gradient solar ponds may be the best mean to capture and store solar energy especially for a relatively long period in thermal form and at lower cost. A solar pond consists of three zones as illustrated in Figure 1.

(a) An upper convection zone (UCZ) of low and uniform concentration, its upper surface constitutes an interface between the air and the water of the pond.
(b) A temperature gradient zone and salinity located in sandwich between the upper zone and the lower zone. In this zone the temperature and salinity increase almost linearly in the direction of the basin depth. This zone is considered as a transparent thermal insulator.
(c) A lower convective zone (LCZ) or the heat storage zone with salinity and temperature relatively high and uniformly distributed. The bottom of this zone is painted black to have a maximum absorption coefficient. It is from this zone that the heat is extracted through hot water and sent towards the exchangers for various applications such as air conditioning, power generation, desalination, etc..

In most studies solar ponds modeling is carried out using one-dimensional mathematical model, in other words, the heat diffusion is assumed only in the vertical direction while keeping the temperature along a layer constant. But, in our case, both the diffusion of horizontal and vertical heat were taken into account and the results of numerical simulation have shown that the difference of the temperature within the same layer of NCZ is significant and can reach 5° C during one season. This result shows the important role of three-dimensional modeling in solving the problem numerically. It should be noted that the experimental solar

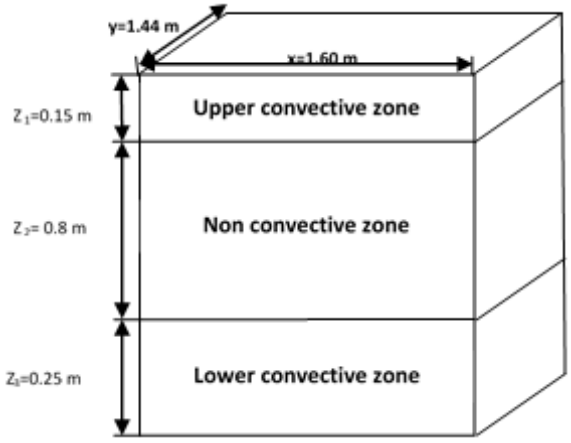

FIGURE 1. Diagram representing the three zones that make up the solar pond

pond located at the coordinates $36°54'15'$ North and $7°45'07$ east, and having a surface of 10000 m^2 with a depth of 2 m, dug into the ground.

It should be noted, by the way, that the non-homogenization of the saline solution leads to a dilatation that can act with force on the internal walls of the solar pond, as well as the non-uniform double extraction leads to an internal flow problem, which allowed us to introduce new parameters of the mechanism. It is also important to point out that for real large-scale solar ponds, the penetration,of solar rays is maximum because of their large surface area which hardly favor any shade, while for experimental ponds, the degree of shading is rather large because of the inclination of the sun, which negatively affects the penetration of the amount of solar radiation reaching the bottom of the basin. The main reason why we had to go to the numirical simulation of large ponds instead of small ponds. Our work consists of modeling the influence of wind on a solar pond when the water is clear, medium-turbid and very turbid, over a period of 30 days, coordinated $36°54'15$ North, $7°45'07$ East and of size (100m $\times 100$m $\times 2$m). The mathematical model proposed is represented by the three-dimensional spatial heat conduction equation with an energy source outside the system but subject to wind stress. An average temperature and insolation values for the last twenteen were obtained using the data provided by Annaba saline station. The numerical resolution approach of the mathematical model adopted is based on the discretization of the heat equation using the finite difference method in conjunction with

the douglas-Gunn scheme, Adams Bashford and Shneider et al with initial and boundary conditions. The essential contribution of this work to the study of a solar pond is to analysis of transient thermal behavior, within the non-convective pond area (NCZ) was conducted through a three-dimensional numerical simulation study based on the coupling of three different techniques: the Douglas-Gunn method, Adams Bashford for linear case resolution, and the Shneider et al technique, which is intended to resolve cases non-linear stationary to make it for transitional non-linear cases. It should be noted that these different digital techniques adopted are recommended in the resolution of the three-dimensional parabolic equations because their stability is good thus allowing several points to be given and their numerical solutions are simpler compared with the traditional Crank-Nicolson method which results in a very complex set of equations whose cost is very high.

2. MATHEMATICAL FORMULATION OF THE PROBLEM

2.1. **Assumptions.** The developed model depends on the following assumptions:

(1) Thermophysical properties such as specific heat C_p, the thermal conductivity k and the density ρ vary from one layer to another.
(2) Turbidity is assumed to be uniform.
(3) The attenuation of solar radiation within the basin is described by the model of Wang and Yagoobi [4].
(4) A statistical average of wind speed and solar radiation was taken into consideration in the last ten years from weather data.
(5) Air and soil temperatures are equal to ambient temperature.

In order to improve the thermal performance of the solar pond, it is essential to study the effect of water turbidity because it has a direct influence on the quantity of radiation reaching the storage zone LCZ. There are few works done on the effect of turbidity. Hull in 1989 [3], in his work on the effect of turbidity on the performance of the basin, showed that the presence of solid particles, microorganisms and their proliferation is harmful because they drastically reduce the transparency of the water of the pond and therefore the performance of the basin. Wang and Yagoobi in 1995 [4] considered the effect of water turbidity on the thermal performance of a solar pond and they proposed an empirical correlation which takes

into account the effect of water turbidity on solar radiation penetration. Nan Li et al. [6] were interested in the control of the turbidity and specifically in microorganisms that can proliferate in high salinity water. They studied the effectiveness of the Alum $KAl(SO_4)_2$ and $12\,H_2O$ to reduce the proliferation of microorganisms in the brine extracted from the seawater desalination unit. Different salts have been used for the purpose of comparing their behavior against the turbidity in a study conducted by Malik et al. (2011) [7]. They used a bittern which is a mixture of NaCl and $MgCl_2$. It is important to note that almost all research dealing with turbidity in solar ponds consider the transient thermal behavior is 1D [4]. In other words, the heat transfer occurs only in the depth direction, but, unfortunately, these models do not reflect real cases of solar ponds where the heat diffusion occurs in the three directions. The 3D heat conduction equation of a solar pond transient thermal behavior was solved numerically by Ben Mansour and Alimi [8]. However, in their work, they used the famous software Fluent in which the resolution is based on the finite volume method despite the simple geometric shape of the solar pond (parallelipedic shape); so in their work one cannot see the details of the numerical resolution steps. In addition, the mathematical model that they applied remains very far from reality especially because of the nonrealistic boundary conditions at the pond walls where the insulation was considered as perfect. Also the simple and inaccurate solar radiation attenuation model does not take into account the turbidity level. In order to distinguish the present work from the problematic of reference [14], we display below a brief overview of the latter followed by the statement of the main objectives of our study.

- Three solar ponds containing three different salts have been investigated and a comparative study has been made.
- A 2D mathematical model was adopted to give the temperature field variation in both directions x and z within the solar pond for three different salts (NaCl, $CaCl_2$ and Na_2CO_3).
- The discretization method used was the 2D Crank-Nicolson scheme where we had employed only a one discretization step. The attenuation model of the solar radiation in the pond is the Rabl-Nilson model which does not take into account the turbidity effect.

- The obtained results showed that the most efficient among the three investigated salts is the calcium chloride ($CaCl_2$). Therefore it records the highest temperature field with respect to other salts. This result could be explained by the low specific heat per unit volume of this salt solution.
- In addition, the heat losses at the vertical walls along the Y axis have been neglected in order to get a simplified 2D mathematical model. But, this simplification although more accurate than the 1D model used by most authors still remains incomplete, so a 3D model is needed to describe the real phenomena.

We note that among the most important factors hindering the operational cost of solar ponds is essentially the turbidity that has a negative influence on the thermal performance of the solar pond. It should be remarked that generally in solar ponds, the sodium hypochlorite is often used to destroy microorganisms which can perturbate the clarity of water pond thus impeding the penetration of solar radiation. We therefore mention that the aim of this study is twofold:

First, we would like to fill the gap encountered in the specialized scientific literature dealing with mathematical modeling in the salinity gradient solar ponds.

Second, to improve their thermal efficiency for practical purposes. A new pond is being investigated with three levels of turbidity and containing one single salt. This constitutes an originality of this work which shows two aspects:

- A practical aspect represented by increasing the amount of penetrating solar radiation using a new fungicide salt.
- The second aspect is focused on improving the 1D and 2D models by introducing the 3D mathematical modeling of the pond with a more precise approach taking into account the reality of the involved phenomena where the boundary conditions are also more realistic. In addition, the model has been solved using the 3D Douglas-Gunn ADI scheme [9] for the first time in the study of solar ponds. A different solar radiation attenuation model that takes into account the turbidity level in the pond is also being considered.

Moreover, in the present work a better solution is proposed to enhance the clarity of the water by injecting a solution of a fungicide salt (monopotassium phosphate, KH_2PO_4). This salt has a property to eliminate the microorganisms growth and

then favors a large improvement in the clarity of the water. The proposed salt promotes maximum penetration of solar radiation and therefore a rise in temperature at the thermal energy storage zone (LCZ). It is also important to note that, in almost all modeling of solar ponds, heat losses near the vertical walls are not considered. Unfortunately, these models are still far from reality especially when we know that the water in the bottom of the pond can reach a temperature that is three times or more the temperature of the ground or of the walls, showing that the walls are a major heat sink absorption.

In order to represent the problem with accuracy, a 3D mathematical model has been developed with an initial condition and six realistic types of boundary conditions. The present study considers a relatively larger area of 2.3040 m^2 than that used experimentally in our previous work of 1 m^2 [14] allowing better solar radiation collection resulting in higher thermal efficiency operation. This work is the study of the evolution of the temperature field in spatial directions based on two different approaches, namely: The first is to simulate numerically over a period of 30 days three solar ponds of identical geometry size (1.6 m $\times 1.44$m $\times 1.2$m). Each pond contains the same salt (KH_2PO_4) but with different turbidity levels: relatively clear water, slightly turbid water and very turbid water, under the same climatic conditions of Annaba city (Algeria) with coordinates $36°54'15$ North, $7°45'07$ East. The second is devoted to the validation of numerical results by conducting an experiment on the same ponds described above. The proposed mathematical model is represented by the 3D heat conduction equation with a source of generation of energy. An average temperature and insolation values for the last twenty years were obtained using the data provided by Annaba saline station. The numerical resolution approach adopted is based on the discretization of the heat equation using the finite difference method in conjunction with the Douglas-Gunn ADI scheme [9] with an initial condition and six boundary conditions. The main contribution of the present work related to the study of a solar pond lies in:

i. The analysis of the transient thermal behavior within the non-convective zone (NCZ) of the pond was realized through a 3D numerical simulation study based on the Douglas-Gunn ADI method that finds its first application in a salinity gradient solar pond. It should be emphasized that this

implicit three steps scheme is recommended for solving 3D parabolic partial differential equations because its stability is better compared to the explicit schemes. Furthermore, its numerical solution is simpler compared to the Crank-Nicolson method which leads to a very complex set of equations whose computational cost is very expensive.

ii. For the first time, an experiment on three small ponds was carried out containing a fungicide salt namely monopotassium phosphate but with three different levels of turbidity. It should be emphasized that this salt has never been used before in solar ponds and, having a destructive power against fungicide, enhances the clarity and transparency of the water. Therefore this salt decreases the turbidity due to the presence of microorganisms and hence allowing better penetration of sunlight.

2.2. **Mathematical formulation.**

2.2.1. *Boundary conditions.* $z1$, $z2$ and $z3$ are given in Figure 1.

i. At $z = z_1$,

$$T(x, z_1, t) = T_a. \tag{2.1}$$

ii. At the interface $z = z_1 + z_2$, the temperature is calculated on the basis of energy balance applied to the LCZ:

$$z_3 C_p \frac{\partial T}{\partial t} = -k\frac{\partial T}{\partial z} + E_{\text{LCZ}} - Q_{\text{out}}, \tag{2.2}$$

where E_{LCZ} represents the insolation entering the storage zone LCZ and Q_{out} represents the heat loss from the storage zone LCZ.

iii. At $x = 0$ and $y = 0$,the temperature is computed from the following equations respectively

$$-k\frac{\partial T}{\partial x}\bigg|_{(x=0)} = C_{ht}(T - T_a)\ , \tag{2.3}$$

$$-k\frac{\partial T}{\partial x}\bigg|_{(y=0)} = C_{ht}(T - T_a). \tag{2.4}$$

iv. At $x = L_1$ and $y = L_2$ the temperature is computed from the following equations respectively:

$$-k\frac{\partial T}{\partial x}\bigg|_{(x=L_1)} = C_{ht}(T - T_a)\ , \tag{2.5}$$

$$-k\frac{\partial T}{\partial x}\bigg|_{(y=L_1)} = C_{ht}(T - T_a), \tag{2.6}$$

where C_{ht} is the heat transfer coefficient by free convection at the wall towards the surrounding air; this coefficient is estimated to be around $20W/m^{2\cdot\circ}C$ [12]. k represents the thermal conductivity of the water.

3. DISCRETIZATION OF THE PROBLEM

$$\begin{aligned}\frac{T^{n+1}-T^n}{\Delta t} &= \frac{1}{\rho C_p}\left[\frac{\partial}{\partial x}\left(k\frac{\partial T}{\partial x}\right)+\frac{\partial}{\partial y}\left(k\frac{\partial T}{\partial y}\right)+\frac{\partial}{\partial z}\left(k\frac{\partial T}{\partial z}\right)\right]\\ &- \frac{S}{\rho C_p}-\frac{1}{\rho C_p}\left(\mu\frac{\partial T}{\partial x}+\nu\frac{\partial T}{\partial y}+w\frac{\partial T}{\partial z}\right),\end{aligned}$$

where n represented the old time and $n+1$ the new time. Let's introduce the intermediate time $n+\frac{1}{2}$ we have:

$$\frac{T^{n+1}-T^{n+\frac{1}{2}}}{\Delta t} = \frac{1}{\rho C_p}\left[\frac{\partial}{\partial x}\left(k\frac{\partial T}{\partial x}\right)+\frac{\partial}{\partial y}\left(k\frac{\partial T}{\partial y}\right)+\frac{\partial}{\partial z}\left(k\frac{\partial T}{\partial z}\right)\right]-\frac{S}{\rho C_p} \tag{3.1}$$

$$\frac{T^{n+\frac{1}{2}}-T^{n}}{\Delta t} = \frac{1}{\rho C_p}\left(\mu\frac{\partial T}{\partial x}+\nu\frac{\partial T}{\partial y}+w\frac{\partial T}{\partial z}\right). \tag{3.2}$$

Equation (3.1) represents the diffusion contribution and Equation (3.2) represents the convective transport.

Let's apply the third order Adams-Bashforth time stepping scheme to Equation (3.2),

$$\begin{aligned}&\frac{T^{n+\frac{1}{2}}-T^n}{\Delta t}\\ &= \frac{-23}{12}\left(\mu\frac{\partial T}{\partial x}+\nu\frac{\partial T}{\partial y}+w\frac{\partial T}{\partial z}\right)^{n+\frac{1}{3}}+\frac{4}{3}\left(\mu\frac{\partial T}{\partial x}+\nu\frac{\partial T}{\partial y}+w\frac{\partial T}{\partial z}\right)^{n+\frac{1}{6}}\\ &- \frac{5}{12}\left(\mu\frac{\partial T}{\partial x}+\nu\frac{\partial T}{\partial y}+w\frac{\partial T}{\partial z}\right)^{n}.\end{aligned}$$

In order to discretize the Equation 3.1 let us introduce the intermediate time $n+\frac{3}{4}$ we will have

Linear case:

$$\frac{T^{n+1}-T^{n+\frac{3}{4}}}{\Delta t} = \frac{1}{\rho C_p}\left(k\frac{\partial T^2}{\partial x^2}+k\frac{\partial T^2}{\partial y^2}+k\frac{\partial T^2}{\partial z^2}\right)-\frac{S}{\rho C_p} \tag{3.3}$$

Nonlinear case:

$$\frac{T^{n+\frac{3}{4}} - T^{n+\frac{1}{2}}}{\Delta t} = \frac{1}{\rho C_p}\left(\frac{\partial k}{\partial x}\frac{\partial T}{\partial x} + \frac{\partial k}{\partial y}\frac{\partial T}{\partial y} + \frac{\partial k}{\partial z}\frac{\partial T}{\partial z}\right) \tag{3.4}$$

In order to solve Equation 3.3 which is parabolic, we have applied the method ADI (Alternating Direction Implicit) because it is well suited to the resolution of the parabolic equation, unconditionally stable and convergent and has quadratic order of convergence.

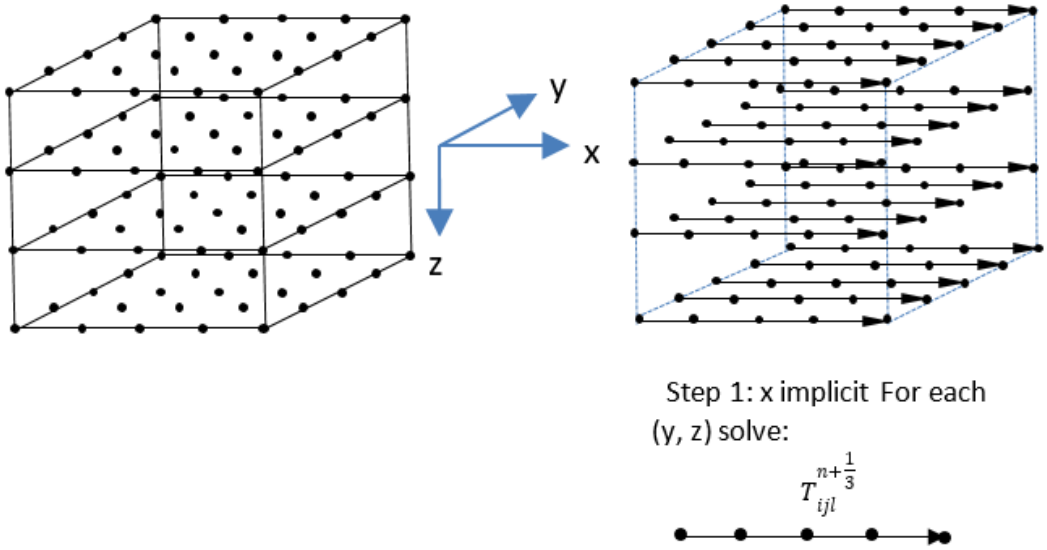

FIGURE 2. Mesh representation for the 3 space discretisation steps $\Delta x = \Delta y = \frac{1}{4}$ and $\Delta z = \frac{1}{3}$ corresponding to three time substeps $\Delta t = \frac{1}{3}$ by applying the ADI Douglas-Gunn scheme.

To overcome this disadvantage and in order to have an unconditional stability with quadratic convergence order, Douglas and Gunn [9] developed a numerical technique based on the improvement of the Peaceman-Rachford ADI scheme [13] by dividing the time step in 3 subtime steps (Figure 2). So this method known as splitting is intended to solve the 3D parabolic partial differential equations. This method falls into the category of fractional step methods [9]. We advance with one third of the step for every iteration to follow the evolution of the temperature field. The nice feature of this method is the simplicity of the obtained system of equations which can be solved efficiently in each substep by Thomas tridiagonal

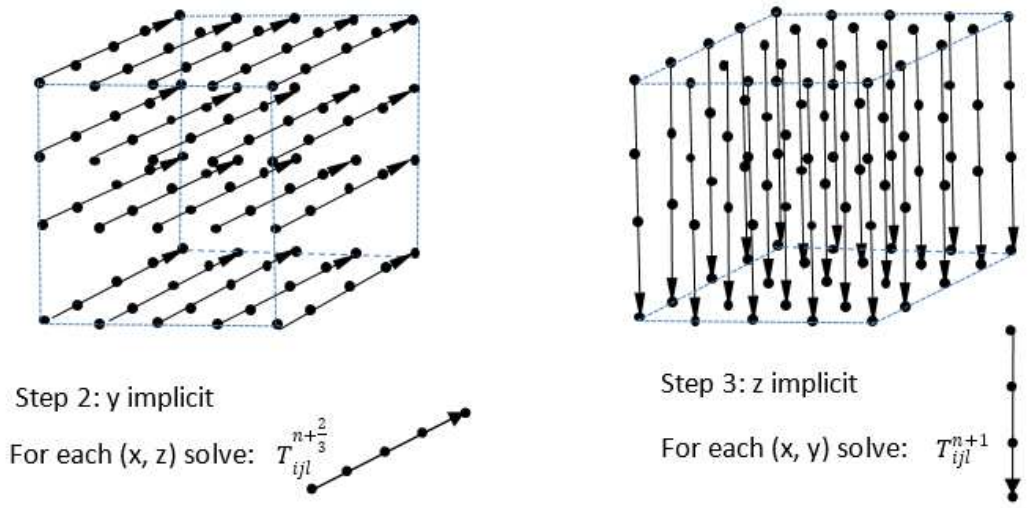

FIGURE 3

matrix algorithm [9]. Dividing the x spatial domain $[0, L_1] = [0, 100m]$ into M sections having each a length of $\Delta x = \frac{L_1}{M} = \frac{100m}{M}$, the y spatial domain $[0, L2] = [0, 100m]$ into N sections having each a length of $\Delta y = \frac{L_2}{N} = \frac{100m}{N}$ and the z spatial domain $[0, L_3] = [0, 2.40m]$ into P sections having each a length of $\Delta z = \frac{L_3}{P} = \frac{2.40m}{P}$. The time domain $[0, T] = [0, 30days]$ is divided into Q segments, each of duration $\Delta t = \frac{T}{Q} = \frac{30days}{Q}$. Letting $x_i = i\Delta x$ for $i = 1, 2, \ldots, M, y_j = j\Delta y$ for $j = 1, 2, \ldots, N, Z_l = l\Delta Z$ for $l = 1, 2, \ldots, P$ and $t_n = n\Delta t$ for $n = 1, 2, \ldots, Q$, therefore Equation (3.3) can be rewritten as follows:

$$\begin{aligned} T^{n+1} - T^{n+\frac{3}{4}} = \quad & \frac{k\Delta t}{2\rho C_p}\frac{\partial_x^2}{(\Delta x)^2}\left(T^{n+1} + T^{n+\frac{3}{4}}\right) + \frac{k\Delta t}{2\rho C_p}\frac{\partial_y^2}{(\Delta y)^2}\left(T^{n+1} + T^{n+\frac{3}{4}}\right) \\ & + \frac{k\Delta t}{2\rho C_p}\frac{\partial_z^2}{(\Delta z)^2}\left(T^{n+1} + T^{n+\frac{3}{4}}\right) + \frac{\Delta T}{\rho C_p}\frac{dE}{dZ}, \end{aligned}$$

with the notation:

$$\begin{aligned} \partial_x^2 T^{n+1} &= T_{i-1,j,l}^{n+1} - 2T_{i,j,l}^{n+1} + T_{i+1,j,l}^{n+1} \\ \partial_y^2 T^{n+1} &= T_{i,j-1,l}^{n+1} - 2T_{i,j,l}^{n+1} + T_{i,j+1,l}^{n+1} \\ \partial_z^2 T^{n+1} &= T_{i,j,l-1}^{n+1} - 2T_{i,j,l}^{n+1} + T_{i,j,l+1}^{n+1}, \end{aligned}$$

$\partial_x^2, \partial_x^2$ and ∂_x^2 are the central difference operators in x, y and z direction respectively.

Putting $r_x = k\Delta t/(\rho C_p \Delta x^2)$, $r_y = k\Delta t/(\rho C_p \Delta y^2)$ and $r_z = k\Delta t/(\rho C_p \Delta z^2)$, we get:

$$\begin{aligned} T^{n+1} - T^{n+\frac{3}{4}} &= r_x \frac{\partial_x^2}{2}\left(T^{n+1} + T^{n+\frac{3}{4}}\right) + r_y \frac{\partial_y^2}{2}\left(T^{n+1} + T^{n+\frac{3}{4}}\right) \\ &+ r_z \frac{\partial_z^2}{2}\left(T^{n+1} + T^{n+\frac{3}{4}}\right) + \frac{\Delta T}{\rho C_p}\frac{dE}{dZ}, \end{aligned} \tag{3.5}$$

Instead of directly solving (3.5) at every time step n, we solve the same equations for three subtime steps for each time step n.

We give below the description of each subtime step.

Step 1:

$$T^{n+\frac{5}{6}} - T^{n+\frac{3}{4}} = r_x \frac{\partial_x^2}{2}\left(T^{n+\frac{5}{6}} + T^{n+\frac{3}{4}}\right) + r_y \partial_y^2 T^{n+\frac{3}{4}} + r_Z \partial_Z^2 T^{n+\frac{1}{2}} + \frac{\Delta T}{\rho C_p}\left[\frac{dE}{dt}\right]^n \tag{3.6}$$

Step 2:

$$\begin{aligned} T^{n+\frac{11}{12}} - T^{n+\frac{3}{4}} &= r_x \frac{\partial_x^2}{2}\left(T^{n+\frac{5}{6}} + T^{n+\frac{3}{4}}\right) + r_y \frac{\partial_y^2}{2}\left(T^{n+\frac{11}{12}} + T^{n+\frac{3}{4}}\right) \\ &+ r_Z \partial_Z^2 T^{n+\frac{3}{4}} + \frac{\Delta T}{\rho C_p}\left[\frac{dE}{dt}\right]^{n+\frac{5}{6}} \end{aligned} \tag{3.7}$$

Step 3:

$$\begin{aligned} T^{n+\frac{11}{12}} - T^{n+\frac{3}{4}} &= r_x \frac{\partial_x^2}{2}\left(T^{n+\frac{5}{6}} + T^{n+\frac{3}{4}}\right) + r_y \frac{\partial_y^2}{2}\left(T^{n+\frac{11}{12}} + T^{n+\frac{3}{4}}\right) \\ &+ r_Z \frac{\partial_Z^2}{2}\left(T^{n+1} + T^{n+\frac{3}{4}}\right) + \frac{\Delta T}{\rho C_p}\left[\frac{dE}{dt}\right]^{n+\frac{11}{12}}. \end{aligned} \tag{3.8}$$

In this work we will introduce two parameters, the dilation β and the vortex ω, which they are strongly depend on the velocity field by the following relations:

$$rotV = \omega, \quad divV = \beta, \quad \{\nabla^2 V = \beta - rot\omega\}.$$

Note that the dilation represents a force called source-like acting strongly on the vertical and horizontal walls of the pond, while the vortex acts strongly on the stratified salt layers and having the role of destroying the stability of the pond.

The discretization of Equation (3.4) gives:

$$\begin{aligned} T_{i,j,l}^{n+\frac{3}{4}} &= \frac{\Delta t}{\rho C_p}\left[\frac{K_{i-\frac{1}{2},j,l}}{(\Delta x)^2}T_{i-1,j,l}^{n+\frac{1}{2}} + \frac{K_{i,j-\frac{1}{2},l}}{(\Delta y)^2}T_{i,j-1,l}^{n+\frac{1}{2}} + \frac{K_{i,j,l-\frac{1}{2}}}{(\Delta z)^2}T_{i,j,l-1}^{n+\frac{1}{2}}\right] \\ &+ \left[1 - \frac{\Delta t}{\rho C_p}\left(\frac{K_{i+\frac{1}{2},j,l}}{(\Delta x)^2} + \frac{K_{i,j+\frac{1}{2},l}}{(\Delta y)^2} + \frac{K_{i,j,l+\frac{1}{2}}}{(\Delta z)^2} + \frac{K_{i-\frac{1}{2},j,l}}{(\Delta x)^2}\right.\right. \\ &+ \left.\left.\frac{K_{i,j-\frac{1}{2},l}}{(\Delta y)^2} + \frac{K_{i,j,l-\frac{1}{2}}}{(\Delta z)^2}\right)\right] T_{i,j,l}^{n+\frac{1}{2}} + \frac{\Delta t}{\rho C_p}\left[\frac{K_{i+\frac{1}{2},j,l}}{(\Delta x)^2}T_{i+1,j,l}^{n+\frac{1}{2}}\right. \\ &+ \left.\frac{K_{i,j+\frac{1}{2},l}}{(\Delta y)^2}T_{i,j+1,l}^{n+\frac{1}{2}} + \frac{K_{i,j,l+\frac{1}{2}}}{(\Delta z)^2}T_{i,j,l+1}^{n+\frac{1}{2}}\right] \end{aligned}$$

4. NUMERICAL RESOLUTION

4.1. **Systems of equations.** Using step 1 in Equation (3.6), we solve numerically the model by fixing j and l and varying i from 1 to M, we therefore get a simple system of linear equations with a tridiagonal structure. The first system has as unknowns the temperature at time $n + \frac{1}{3}$ that will be solved as a function of temperature at time n. The second system comes from step 2 and Equation (3.7) has as unknowns the temperature at time $n + \frac{2}{3}$ that will be solved as a function of temperature at times n and $n + \frac{1}{3}$, and the third system derives from Equation (3.8) and includes as unknowns the temperature at time $n+1$ which will be solved as a function of the temperature at times $n + \frac{1}{3}$, $n + \frac{2}{3}$ and n.

4.2. **Implementation of the initial and boundary conditions.** We give below the discretization of the boundary conditions:

- at the pond water surface, the temperatures $T_{i,j,0}^{n+1}$, for $i = 1, 2, \ldots, M, j = 1, 2, \ldots .N$, are calculated by the 1st boundary condition in Equation (2.1).
- at the interface $z = z_1 + z_2$ corresponding to $l = P$, the discretization of the Equation (2.2) for $i = 1, 2, \ldots, M$ and $j = 1, 2, \ldots, N$ gives:

$$T_{i,j,l+1}^{n+\frac{1}{3}} = T_{i,j,l+1}^{n}\left[1 - \frac{k\Delta t}{\rho C \rho \Delta z Z_3}\right] + \frac{k\Delta t T_{i,j,l}^{n}}{\rho C \rho \Delta z Z_3} + \frac{(E_{\text{LCZ}} - Q_{\text{out}})\Delta t}{Z_3 C_P}.$$

In our case $T^n_{i,j,l+1} = T^n_{i,j,l}$ since the temperature of the LCZ is equal to the temperature of the last layer NCZ. Q_{out} represents about 14% of the incident energy [14].

- At $x = 0$ corresponding to $i = 1$, the discretization of the Equation (2.3) gives:
$$T^{n+\frac{1}{3}}_{0,j,l} = \frac{k}{k - C_{ht}\Delta x}\left(T^{n+\frac{1}{3}}_{1,j,l}\right) - \left(\frac{C_{ht}\Delta x T_a}{k - C_{ht}\Delta x}\right).$$
- At $x = L_1$ corresponding to $i = M$ the discretization of the Equation (2.5) gives:
$$T^{n+\frac{1}{3}}_{M+1,j,l} = \left(\frac{k - C_{ht}\Delta x}{k}\right)\left(T^{n+\frac{1}{3}}_{M,j,l}\right) + \left(\frac{C_{ht}\Delta x T_a}{k}\right).$$
- At $y = 0$ corresponding to $j = 1$, we obtain after the discretization of the Equation (2.4):
$$T^{n+\frac{2}{3}}_{i,0,l} = \left(\frac{k}{k - C_{ht}\Delta y}\right)\left(T^{n+\frac{2}{3}}_{i,1,l}\right) - \left(\frac{C_{ht}\Delta y T_a}{k - C_{ht}\Delta y}\right).$$
- At $y = L_2$ corresponding to $j = N$, we obtain after the discretization of the Equation (2.6):
$$T^{n+\frac{2}{3}}_{i,N+1,l} = \left(\frac{k - C_{ht}\Delta y}{k}\right)\left(T^{n+\frac{2}{3}}_{i,N,l}\right) + \left(\frac{C_{ht}\Delta y T_a}{k}\right).$$

Finally, by adopting the same reasoning for step 2 and step 3, we obtain three linear systems of equations where the matrix in each system is tridiagonal. The MATLAB [R2006a] of LANOS laboratory has been used for the numerical solution.

5. EXPERIMENTAL PROCEDURE

5.1. **Establishment of salinity gradient and turbidity.** Three galvanized steel, parallelepiped shaped experimental basins with an area of 1.6 x 1.44 m and a depth of 1.2 m were used to perform the experiments. Each basin contains the same salt namely KH_2PO_4. The walls are not insulated; the pond bottom is black painted to enhance solar radiation absorption. Four different solutions with their salt concentrations $(6\%, 12\%, 18\%$ and $24\%)$ have been carefully prepared in the laboratory and are poured gradually with a plastic diffuser to ensure a perfect stratification to avoid turbulence causing layer mixing. Concerning slightly turbid and very turbid pond, the water used is extracted from stagnant lakes in two

different places of Annaba city to ensure that they are natural and contain all kinds of factors causing turbidity such as microorganisms, algae and particles. It should be noted that the three different turbidity levels used in this experiment are: $\Theta = 0.5$ NTU for relatively clear water. $\Theta = 1.5$ NTU for an slightly turbid water. $\Theta = 4$ NTU for a very turbid water. The thicknesses of the three zones of every experimental basin are given as follows: $0,15$ m for the upper zone UCZ. $0,80$ m for the non convective zone NCZ which in turn is divided into 4 layers of 0.20 m each, $0,25$ m for the storage area whose LCZ.

5.2. **Measurement procedure.** To measure temperatures in the non-convective zone NCZ, 5 thin transparent plastic strips, each one containing 16 thermocouples were installed according to the following locations:

(1) One strip S_1 is in the center of the basin along the vertical line.
(2) Four other remaining strips S2, S3, S4 and S5 are located in the vertical central line of the four side walls of the basin in the vertical direction (see Fig 4).

Temperatures are recorded every two hours for a period of 30 days using a DATA-LOGGER manufactured in the laboratory. A digital thermometer outside the solar pond is used to follow the changes in the ambient temperature of the site.

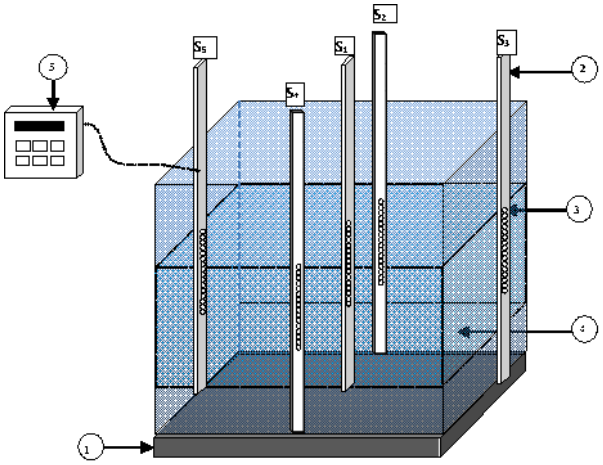

FIGURE 4. Experimental setup of the SGSP: 1- bottom of the pond, 2- strip, 3- thermocouples position, 4- stratified solutions, 5- Data-logger

6. RESULTS AND DISCUSSION

6.1. **3D model and temperature profile.** The 3D temperature profiles as function of the different turbidity levels are given by Figure 5.

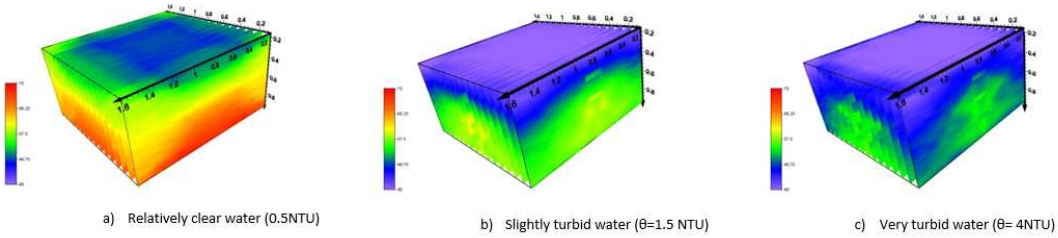

FIGURE 5. 3D temperature profiles visualization for different levels of turbidity: a- Relatively clear water ($\theta = 0.5$ NTU). b- Slightly turbid water ($\theta = 1.5$ NTU). c- Very turbid water ($\theta = 4$ NTU)

It is apparent from Figure 5 that the relatively clear water pond becomes in a short time sufficiently hot to be exploited compared to the other ponds. We first notice that the temperature varies in all three directions as shown in fig 5. This result shows that in real solar ponds the temperature varies in all directions contrary to what have been assumed by many authors who consider that the temper ature varies only along the z depth. For each horizontal plane, the temperature is not the same as shown in Figure 6 which invalidates the main hypothesis of 1D models which assume that the temperature along a horizontal plane is constant.

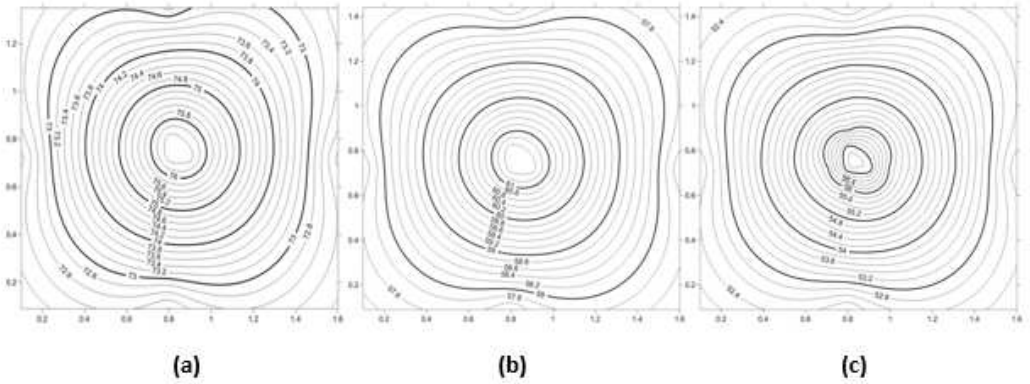

FIGURE 6. Isotherms at section plane $z = 0.8$ m for different levels of turbidity: a) relatively clear water; b) slightly turbid water; c) very turbid water.

The effect of the turbidity level is very apparent in Figures 5 and 6. The higher this level is, the weaker is the radiation penetration power in water and hence the lower is the reached temperature. This is due to the absorption of a part of this radiation by the suspension of minerals or microorganisms. The temperature is higher at the central region of the section at any horizontal plane. For example, at $z = 0.8$ m, the maximum temperature reached is $78.04°C$ for relatively clear water, $60.63°C$ for slightly turbid water and $58.50°C$ for very turbid water. This heating can be also presented as 1D vertical Z temperature profile for every (x, y) coordinates. For example, in the vertical central line (Figure 7) at ($x = 0.8$ m, $y = 0.72$ m) coordinates in the basin, the temperature increases in the z direction attaining a maximum near the bottom. These values are greater, by about $5°C$, than those existing in the vertical walls lines (Figures 8, 9 and 10). Thus confirming the importance of the 3D approach models of real case solar ponds. We must note, in this work, that only the relatively clear water pond had recorded the highest temperature because of the good penetration of solar radiation followed in second place by the slightly turbid water and finally by the pond of very turbid water in third place. Because of the existence of an horizontal temperature difference and under the Soret effect [14], there must exist an horizontal salt migration within the same layer from vertical central line towards the walls. On the other hand, upward vertical salt migration is less important in the center than at the walls, therefore even in LCZ there is more decrease in salt concentration at the walls than at its center and this suggests the location of the right point of salt injection for pond maintenance. This Soret effect causes non uniform upward mass diffusion of salt from LCZ. This would be a factor causing non-uniformity of natural convection flows within LCZ and can negatively affect stability.

6.2. **Comparison between experimental and numerical results.** Case A: relatively clear water (Figure 8) The experimental results of temperature profile in the z direction for the lines A, B and C coincide approximately with the numerical results. The maximum temperatures obtained near the bottom under this condition are: $73.02°C$ corresponding to line A, $74.12°C$ to line B and $78.04°C$ to line C. The rise in temperature is explained by the fact that the solar radiation penetration is so easy because there is no turbidity effect reducing the intensity along the paths within the pond.

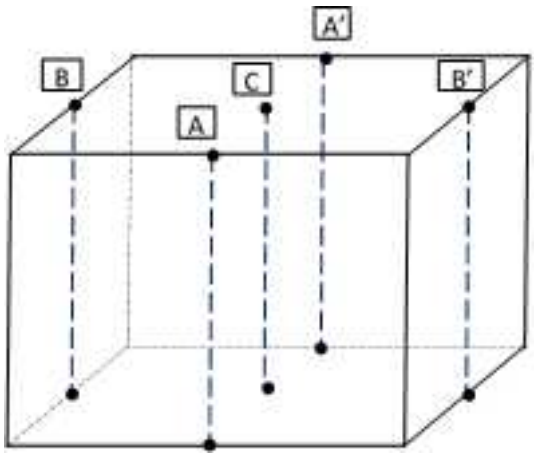

FIGURE 7. Different lines used to compare the temperature variation in z direction (depth): a symmetry in temperature profiles exists between A, A lines; B, B lines.

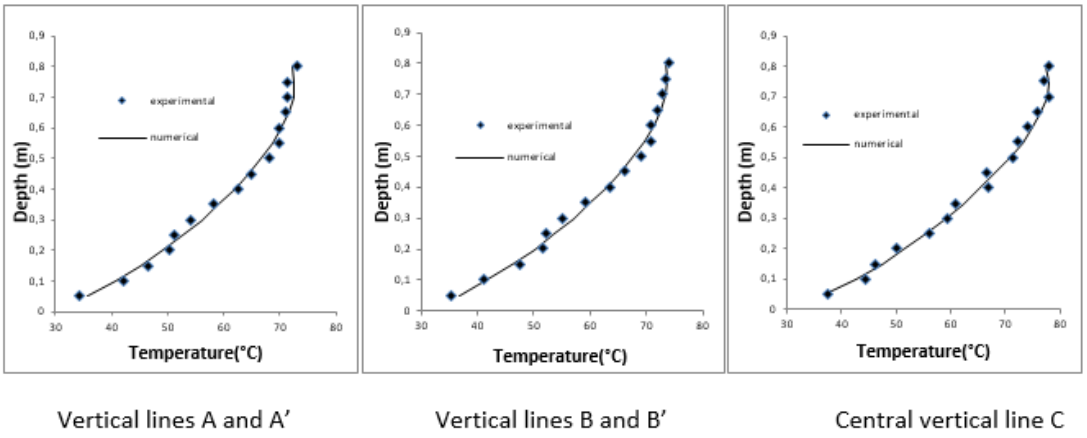

FIGURE 8. Comparison between experimental and numerical temperature variation in z direction (depth) for relatively clear water

Case B: slightly turbid water (Figure 9) In the case of slightly turbid water we distinguish two facts. In the first, we remark that the experimental and numerical curves coincide starting from the top surface of the pond till the middle depth of the pond. However, in the second fact, the curves do not coincide and there is even a divergence as the depth increases. For example, the maximum difference between the two curves can reach $18°C$ as the depth becomes more important.

These two facts mean that the mathematical model is no longer valid in this zone and also underline the clarifying effect of fungicide salt KH_2PO_4 used in the experiment which has the property of destroying microorganisms. It is important to note that the experimental measurements are almost identical to those obtained for the relatively clear water. The experimental temperature reaches also a maximum value near the middle depth then it begins to decrease for greater depth as remarked above in the case of the numerical results. The recorded maximum temperatures are of the order of: $57.56°C$ to line A, $58.22°C$ to line B and $60.63°C$ at line C.

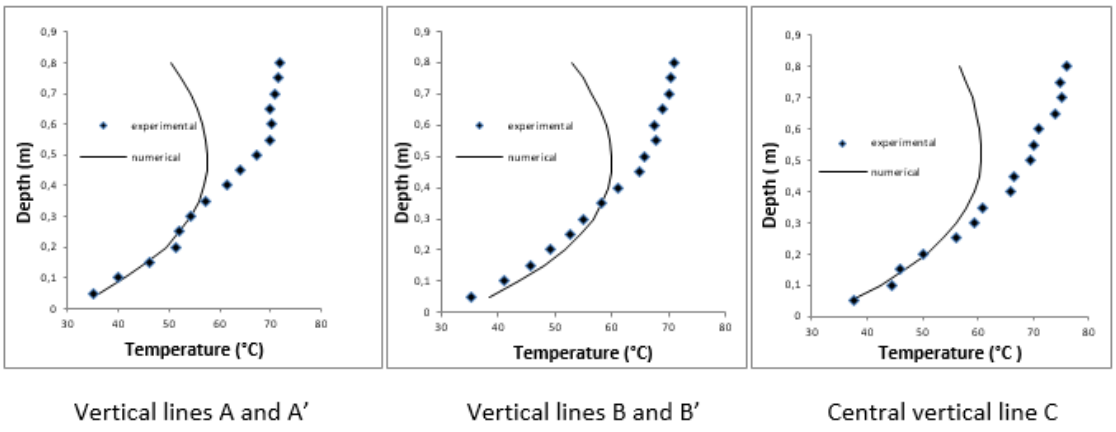

FIGURE 9. Comparison between experimental and numerical temperature variation in z direction (depth) for slightly turbid water.

Case C: very turbid water (Figure 10) We note that the experimental values in this case are almost the same as those of relatively clear water. The numerical model gives a curve that is of the same shape as slightly turbid water which reaches a maximum temperature near the middle of the depth and then begins to decrease for deeper zones. The recorded temperatures are as follows: $55.07°C$ to line A, $55.86°C$ to line B and $58.5°C$ to line C. When the pond water is very turbid, the difference between experimental and numerical temperature values can reach $20°C$. This difference is explained by the fact that the turbidity is caused by the presence of solid particles and microorganisms that find favorable conditions for proliferation. Under gravitation effect, the solid particles deposit in the bottom of the pond where the microorganisms will be killed by the use of fungicide salt

(KH_2PO_4) leaving the pond water relatively clear. Thus allowing maximum penetration of solar radiation reaching the lower convective zone (LCZ) of the pond and therefore increases thermal performance whereas in the numerical model we used $\theta = 4$ NTU for high level turbidity.

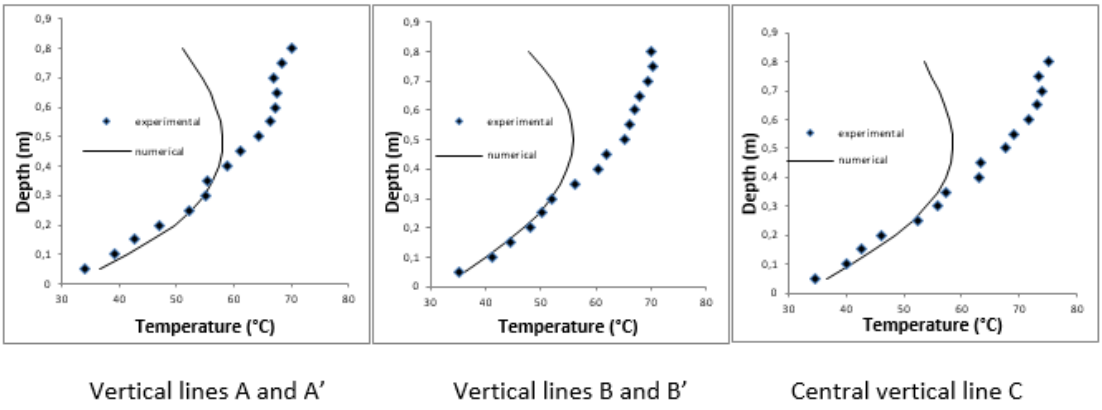

FIGURE 10. Comparison between experimental and predicted temperature variation in z direction (depth) for very turbid water

6.3. **Effect of the space discretization step Δz.** In the present study, we investigate the numerical solution of the parabolic partial differential equation in 3D subject to the above initial and boundary conditions given in subsection 2.2.1. The Douglas-Gunn ADI scheme is being considered because it is stable, accurate and effective but also difficult. A detailed analysis of the Douglas-Gunn ADI scheme for the problem at hand has been given in sections 3 and 4. We recall that the Douglas-Gunn ADI approach for dealing with the 3D heat equation is generally preferred because it results in tridiagonal coefficient matrices which are unconditionally stable, so fewer steps can be performed. Moreover, the overall truncation error of the Douglas-Gunn ADI scheme is second order in both time and space. This is a second factor that allows for fewer steps to be taken with the Douglas-Gunn ADI scheme. The discretization scheme uses four mesh sizes in the three directions namely $16 \times 16 \times 16$, $16 \times 16 \times 32$, $16 \times 16 \times 64$, $16 \times 16 \times 128$. (Figure 11).

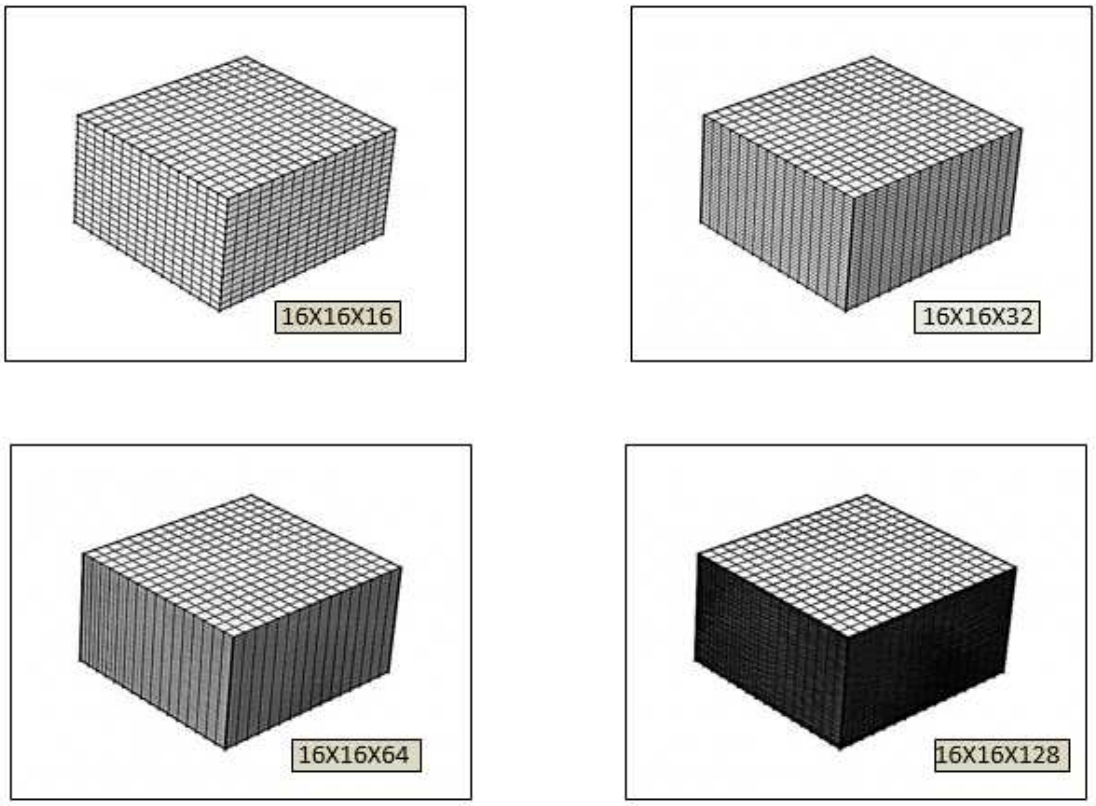

FIGURE 11. Different meshes in the numerical model

We can see that the temperature profiles displayed in (Figure 12) are almost identical. The maximum difference between the temperature profiles along the depth z does not exceed $0.5°C$ which, let us say, means that the numerical results are almost independent of the mesh size adopted (Figure 12).

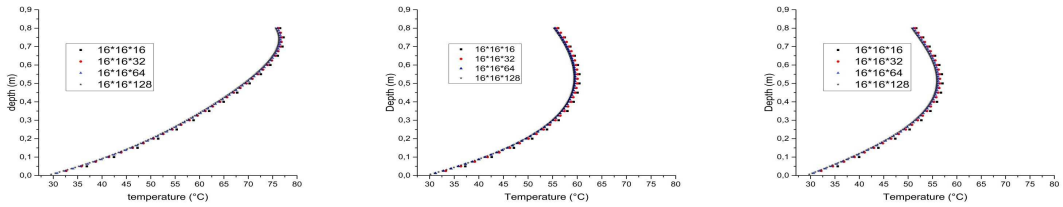

FIGURE 12. Temperature profiles in the central line as function of the discretization step along Z.

6.4. **Numerical validation.** All the numerical calculations given below are related only to the solar pond with relatively clear water as it yields the highest temperature and the most exploitable in thermal applications. In this section we are interested in a numerical verification of the second order accuracy of the Douglas-Gunn ADI scheme in both time and space, i.e., $O(\Delta t^2+\Delta x^2+\Delta y^2+\Delta z^2)$, [15], [16] To this end, let us introduce a reference solution T_{ref} corresponding to the finest size $\Delta z = \frac{0.8}{128}$ and the percentage relative error defined by $\left|\frac{T_{ref}-T_{\Delta z}}{T_{ref}}\right| \times 100$, where $T_{\Delta z}$ is the numerical solution for a given step Δz. We can see from Figure 12 given above that there is a convergence trend of the approximate solutions as the curves become closer when the space steps decrease. Therefore corroborating the theoretical convergence result given by proposition 11.6 of reference [13]. The MATLAB software (v2006a) of the LANOS laboratory has been used on the HP ALTEC computer, CPU Intel core Duo$\times 2, 2.27$ GHz, Memory 2 Gbyte, the CPU time for each nodes number are represented in table 1. In table 1 below, we give the different four mesh sizes together with their corresponding CPU times. It is clear that the CPU time increases as the number of nodes N increases.

TABLE 1. CPU time as function of nodes number

Node Number N		CPU time (sec)
$16 \times 16 \times 16$	(4096)	215.4114
$16 \times 16 \times 32$	(8192)	317.0242
$16 \times 16 \times 64$	(16384)	466.5967
$16 \times 16 \times 128$	(32768)	686.6570

In order to establish the numerical verification of the second order accuracy both in time and space of the Douglas-Gunn ADI scheme, we need to construct table 2 displaying the reference solution and the numerical solutions for different step sizes. We also need to build table 3 containing the absolute errors between the reference solution and the numerical solutions.

Table 2: Comparison between reference and the numerical solutions for different coordinates x, y and z for 3 mesh sizes.

Cordiantes			References solution (C°) $\Delta x = \Delta y = \frac{1}{16}$	Numerical solution (C°) $\Delta x = \Delta y = \frac{1}{16}$		
$x(m)$	$y(m)$	$z(m)$	$\Delta z = \frac{1}{128}$	$\Delta z = \frac{1}{16}$	$\Delta z = \frac{1}{32}$	$\Delta z = \frac{1}{64}$
0.4	0.36	0.8	75.06212	75.52446	75.17194	75.08788
0.4	0.72	0.8	76.66824	77.14291	76.78166	76.69569
0.4	1.08	0.8	75.06212	75.52446	75.17194	75.08788
0.8	0.36	0.8	76.66824	77.14291	76.78166	76.69569
0.8	0.72	0.8	78.04481	78.53872	78.16573	78.07469
0.8	1.08	0.8	76.66824	77.14291	76.78166	76.69569
1.2	0.36	0.8	75.06212	75.52446	75.17194	75.08788
1.2	0.72	0.8	76.66824	77.14291	76.78166	76.69569
1.2	1.08	0.8	75.06212	75.52446	75.17194	75.08788

TABLE 3. Absolute errors for 3 mesh sizes.

Coordinates			Absolute error		
$x(m)$	$y(m)$	$z(m)$	$\Delta z = \frac{1}{16}$	$z = \frac{1}{32}$	$\Delta z = \frac{1}{64}$
0.4	0.36	0.8	0.46234	0.10982	0.02576
0.4	0.72	0.8	0.47467	0.11342	0.02745
0.4	1.08	0.8	0.46234	0.10982	0.02576
0.8	0.36	0.8	0.47467	0.11342	0.02765
0.8	0.72	0.8	0.49391	0.12092	0.02988
0.8	1.08	0.8	0.47467	0.11342	0.02745
1.2	0.36	0.8	0.46234	0.10982	0.02576
1.2	0.72	0.8	0.47467	0.11342	0.02745
1.2	1.08	0.8	0.46234	0.10982	0.02576

The following two tables (table 4 and 5) provide a numerical validation of the Douglas-Gunn ADI scheme in both time and space. Table 4 summarizes the error in the approximate solution at $t = 30$ days for different values of $\Delta x, \Delta y$ and Δz. For all calculations the time step of $\Delta t = \frac{1}{16}$ was used.

TABLE 4. The error in the approximate solution at $t = 30$ days for different values of Δt with $\Delta x = \Delta y = \Delta z = 1/16$.

Mesh size	Maximum absolute error	Error ratio	Root mean square error	Error ratio
$\Delta x = \Delta y = \frac{1}{16}$,$\Delta z = \frac{1}{16}$	0.49391		0.24695	
$\Delta x = \Delta y = \frac{1}{16}$,$z = 1/32$	0.12092	4.08460	0.06046	4.08462
$\Delta x = \Delta y = \frac{1}{16}$, $\Delta z = \frac{1}{64}$	0.02988	4.04685	0.01494	4.04484

TABLE 5. Second order accuracy in time.

Mesh size	Maximum absolute error	Error ratio	Root mean square error	Error ratio
$\Delta t = 30\frac{days}{16}$	0.72865		0.36432	
$\Delta t = 30\frac{days}{16}$	0.17368	4.19565	0.08684	4.19565
$\Delta t = 30\frac{days}{64}$	0.04077	4.25926	0.02038	4.25926

The root mean square (rms) error is given by:

$$\text{rms error} = \sqrt{\frac{1}{Q}\sum_{n=1}^{Q}\left(T_{ref}^{t=30} - T_{n}^{t=30}\right)^2}.$$

We can see from tables 4 and 5 that each reduction in the step size by a factor of two, the error reduces by a factor of four showing the quadratic convergence of the Douglas-Gunn ADI scheme.

REFERENCES

[1] A. AKBARZADEH, G. AHMADI: *Computer simulation of the performance of a solar pond in the southern part of Iran*, Elsevier, Solar Energy, (1980), 143–151.

[2] J. WANG, J. SEYED-YAGOOBI: *Effects of water turbidity and salt concentration levels on penetration of solar radiation under water*, Elsevier, Solar Energy, **56** (1994), 429–438.

[3] J.R. HULL, D.L. BUSHNELL, D.G. SEMPSROTE, A. PENA, A: *Ammonium sulfate solar pond: obser vations from small-scale experiments*, Elsevier, Solar energy, (1989), 57–64.

[4] J. WANG, J. SEYED-YAGOOBI: *Effect of water turbidity on thermal performance of a salt-gradient solar pond*, Elsevier, Solar energy, (1995), 301–308.

[5] M. HUSAIN, P.S. PATIL, S.R. PATIL, S.K. SAMDARSHI: *Optimum size of non-convective zone for improved thermal performance of salt gradient solar pond*, Elsevier, Solar energy, (2003), 429–436.

[6] L.N. HUSAIN, F. YIN, W. SUN, C. ZHANG, , Y. SHI: *Turbidity study of solar ponds utilizing seawater as salt source*, Elsevier, Solar energy, (2010), 289–295.

[7] N. MALIK, A. DATE, J. LEBLANC, A. AKBARZADEH, B. MEEHAN: *Monitoring and maintaining the water clarity of salinity gradient solar ponds*, Elsevier, Solar energy, (2011), 2987–2996.

[8] W. ALIMI: *Simulation numérique 3D du stockage du rayonnement solaire dans un étang solaire*, DEA Thesis, lâĂŹÉNIT, Tunis, Tunisie, (2001), 2987–2996.

[9] T.Y. WANG, C.C.P. CHEN: *3-D thermal-ADI: A linear-time chip level transient thermal simulator*, IEEE, IEEE Transactions on computer-aided design of integrated circuits and systems, (2002), 1434–1445.

[10] R. DARROS-BARBOSA, M. BALABAN, A.A. TEIXEIRA: *Temperature and concentration dependence of heat capacity of model aqueous solutions*,Taylor & Francis, International Journal of Food Properties, (2003), 239–258.

[11] O.N. GRIGOROV, M.E. POZIN: *Chemist reference*,Chemist reference: tome 3 (2nd edition), Mir edition., 1965.

[12] R.H. PERRY, D.W. GREEN, J.O. MALONEY: *Perry's Chemical Engineers' Handbook (ed.)*,Seventh, International edition, 1997.

[13] R.M.M. MATTHEIJ, S.W. RIENSTRA, J.H.M. BOONKKAMP, T. TEN: *Partial differential equations: modeling, analysis, computation*, SIAM, 2005.

[14] B.M. MATTHEIJ, H. SISSAOUI, A. ABDELLI, M. KERMICHE, G. BARKER-READ: *Comparison of three solar ponds with different salts through bi-dimensional modeling*, Solar Energy (2015), 56–68.

[15] L. MATTHEIJ, D. PETER, R.D. RICHTMYER: *Survey of the stability of linear finite difference equations*, Wiley Online Library, Communications on pure and applied mathematics (1956), 267–293.

[16] B. BRADIE: *A friendly introduction to numerical analysis*, Pearson Education India, 2006.

DEPARTMENT OF PREPARATORY CLASS, NATIONAL POLYTECHNIC INSTITUTE OF CONSTANTINE, ALI MENDJELI, CONSTANTINE, ALGERIA.

Email address: bahi.oussama2@gmail.com

DEPARTMENT OF MATHEMATIC, UNIVERSITY OF TAMANRASSET, ANNABA, ALGERIA.

Email address: $abdelli_ammar@yahoo.fr$